Appl Phys A (2014) 114:1009–1016
DOI 10.1007/s00339-013-7673-8

Applied Physics A
Materials Science & Processing

Improving dopant incorporation during femtosecond-laser doping of Si with a Se thin-film dopant precursor

Matthew J. Smith · Meng-Ju Sher · Benjamin Franta · Yu-Ting Lin · Eric Mazur · Silvija Gradečak

Received: 24 January 2013 / Accepted: 14 March 2013 / Published online: 29 March 2013
© Springer-Verlag Berlin Heidelberg 2013

Abstract We study the dopant incorporation processes during thin-film fs-laser doping of Si and tailor the dopant distribution through optimization of the fs-laser irradiation conditions. Scanning electron microscopy, transmission electron microscopy, and profilometry are used to study the interrelated dopant incorporation and surface texturing mechanisms during fs-laser irradiation of Si coated with a Se thin-film dopant precursor. We show that the crystallization of Se-doped Si and micrometer-scale surface texturing are closely coupled and produce a doped surface that is not conducive to device fabrication. Next, we use this understanding of the dopant incorporation process to decouple dopant crystallization from surface texturing by tailoring the irradiation conditions. A low-fluence regime is identified in which a continuous surface layer of doped crystalline material forms in parallel with laser-induced periodic surface structures over many laser pulses. This investigation demonstrates the ability to tailor the dopant distribution through a systematic investigation of the relationship between fs-laser irradiation conditions, microstructure, and dopant distribution.

Electronic supplementary material The online version of this article (doi:10.1007/s00339-013-7673-8) contains supplementary material, which is available to authorized users.

M.J. Smith (✉) · S. Gradečak
Department of Materials Science and Engineering, Massachusetts Institute of Technology, Cambridge, MA 02139, USA
e-mail: mjsmith@mit.edu
Fax: +1-617-2587620

S. Gradečak
e-mail: gradecak@mit.edu
Fax: +1-617-2587620

M.-J. Sher · E. Mazur
Department of Physics, Harvard University, Cambridge, MA 02138, USA

B. Franta · Y.-T. Lin · E. Mazur
School of Engineering and Applied Sciences, Harvard University, Cambridge, MA 02138, USA

1 Introduction

The use of pulsed laser irradiation to dope Si with chalcogens (S, Se, Te) to concentrations orders of magnitude beyond the equilibrium solubility limit results in a drastic increase in both the visible and infrared absorptance of Si [1, 2] and increased gain and extended photoresponse in Si-based photodetectors [3–5]. Doping semiconductors with supersaturated concentrations of deep-level impurities is also a potential route to synthesizing an intermediate band semiconductor, a high-efficiency photovoltaic concept through which single-junction solar cells have theoretical efficiency limits greater than 50 % [6]. As such, there is great interest in the further development of pulsed laser doping as a platform for tailoring the optoelectronic properties of Si.

Pulsed laser doping can be achieved by introducing the dopants as a gas [2, 3, 7–11], a thin film [5, 9, 12, 13], or by ion implantation [4, 14–16], followed by irradiation with pulse lengths ranging from nanoseconds (ns) [4, 11, 14–16] to femtoseconds (fs) [2, 3, 7–12]. The doping of Si using fs-laser irradiation in the presence of SF_6 has been used to fabricate IR photodetectors with responsivities extending down to 0.8 eV [3], and extended photoresponse has also been demonstrated using picosecond pulsed laser irradiation of a Se thin film on Si [5]. Strong increases in sub-band gap absorption can be achieved using ion implantation of chalcogens followed by ns pulsed laser melting [14, 15], but the resulting photodiodes do not exhibit such extended responsivity into the infrared [3, 4]. Both the pulse duration and

method of dopant introduction have a drastic effect on the resulting bulk properties; understanding these relationships is central to advancing pulsed laser doping as a platform for tailoring the optoelectronic properties of Si.

The recent progress in developing femtosecond (fs)-laser doping as a platform for materials synthesis has focused on the irradiation of Si in the presence of SF_6, a gaseous dopant precursor [8, 17, 18]. The deposition of a thin film of material onto the surface prior to pulsed laser irradiation, however, is a low cost approach to introducing dopants and enables doping with elements without available gaseous dopant precursors [5, 16, 19]. The deposition of a chalcogen thin film (Se, Te) followed by fs-laser irradiation has been shown to result in an increase in sub-band gap absorptance comparable to using a gaseous dopant precursor [7, 9]. There has been little success, however, in fabricating devices using a thin-film dopant precursor and fs-laser irradiation, which we have previously attributed to different dopant incorporation and surface texturing processes arising due to the presence of the thin film [12]. The effectively infinite dopant source present in the ambient atmosphere during doping from a gaseous dopant precursor enables the formation of a continuous doped surface layer in parallel with surface texturing. However, fs-laser doping from a thin film produces discontinuous regions of doped material isolated to within polycrystalline surface peaks [12]. Femtosecond laser doping with a thin-film precursor could enable synthesis of a wide range of novel materials, but realizing this potential requires understanding and optimizing the dopant incorporation and surface texturing processes.

In this work, we study the effects of a thin-film dopant precursor on surface texturing and dopant incorporation to enable control of the resulting structure and dopant distribution. We begin our investigation of the surface texturing and dopant incorporation processes during thin-film fs-laser doping by studying the evolution of the surface morphology, microstructure, and dopant distribution with an increasing number of laser pulses. We show that the surface texturing process is directly coupled to the localized crystallization of Se-rich Si on the surface. We then investigate the dopant distribution as a function of laser fluence and demonstrate the synthesis of a continuous, crystalline doped surface layer using irradiation conditions that suppress surface texturing over many laser pulses.

2 Experimental

We investigated thin-film fs-laser doping using a 75-nm thin film of Se thermally evaporated onto a Si wafer as a dopant precursor. Following film deposition, the wafer was loaded into the vacuum chamber and the chamber was evacuated and then backfilled with 500 Torr of N_2. A Ti:sapphire laser ($\lambda = 800$ nm, $\tau = 80$ fs, $f = 100$ Hz) was then used to irradiate Si with 1, 2, 5, 10, 15, 20, 30, 50, and 100 stationary pulses, each with a peak fluence, F, of 4 kJ/m^2. The Gaussian laser beam profile was measured using a CCD camera and has a full-width half-maximum of 343 µm and 436 µm, parallel and perpendicular to the direction of beam polarization, respectively. Understanding the fluence profile allows us to determine the effective fluence at a point within the laser-irradiated spot by measuring the distance to the center of the spot, which we use to study the effect of fluence variation on the surface morphology and dopant incorporation.

The sample morphology was investigated using a FEI Helios 600 scanning electron microscope (SEM) and a Zeiss Field Ultra55 field emission scanning electron microscope (FESEM), both operated at a 5 kV accelerating voltage. To quantify the absolute change in height of the evolving surface morphology, profilometry was performed on each of the laser-irradiated spots using a Veeco Dektak 6M Profilometer. The resulting microstructure and dopant distribution were characterized using a JEOL 2010F transmission electron microscope (TEM) operated at 200 kV. Samples were prepared from specific regions within each stationary laser pulse using the lift-out method on a FEI Helios 600 dual-beam focused ion beam (FIB). We used bright-field (BF) TEM to understand the microstructure and dark-field scanning TEM (DF-STEM) in combination with energy dispersive X-ray spectroscopy (EDX) to map the Se distribution. Because the chemical resolution of EDX is on the order of 1 %, the quantification of EDX spectra presented in this work is only qualitative; EDX is capable only of identifying regions that contain Se concentrations about 3 orders of magnitude above their solubility limit.

3 Results and discussion

3.1 Femtosecond laser doping with laser irradiation in the texturing regime

We first investigate the evolution of the surface texturing and dopant distribution during thin-film fs-laser doping with an increasing number of laser pulses. Using this knowledge, we gain insights into the laser–material interactions relevant to fs-laser doping, including melting and resolidification, dopant incorporation, evaporation, and ablation.

3.1.1 Dopant distribution following 1–5 pulses at F = 4 *kJ/m*^{2}

The laser-material interactions during the initial laser pulses influence dopant incorporation during subsequent pulsed-laser irradiation, and hence we first focus on the effects of a single laser pulse. An SEM image of the center of this spot

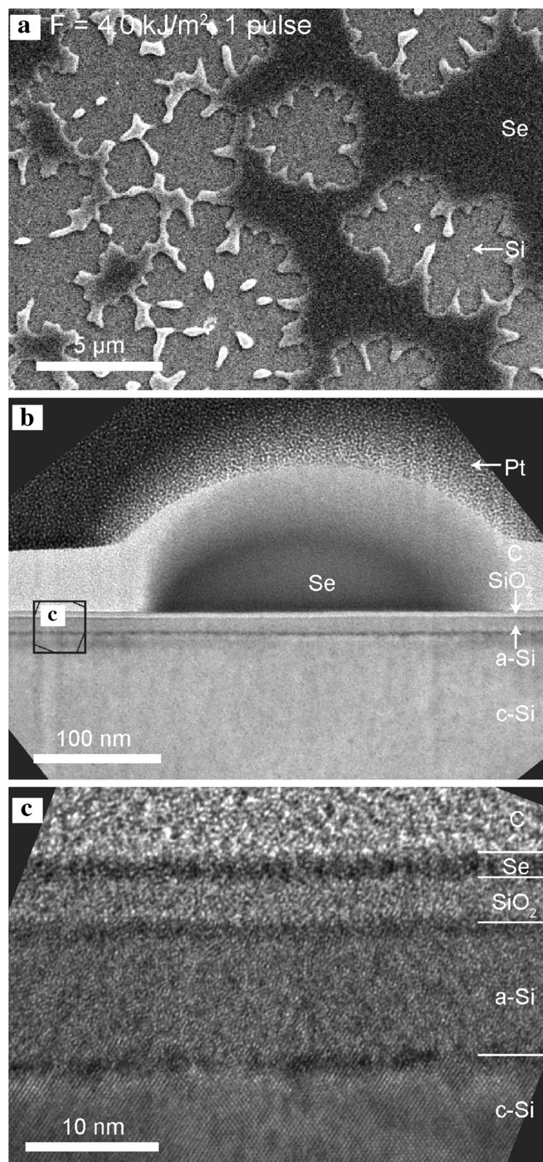

Fig. 1 (**a**) Top-view SEM image of surface after a 4.0 kJ/m^2 fs-laser pulse, showing the discontinuous nature of the Se thin film after a single pulse. (**b**) Bright-field TEM image of silicon surface after a single laser pulse. (**c**) High-magnification TEM of the modified silicon surface, from the region indicated in (**b**)

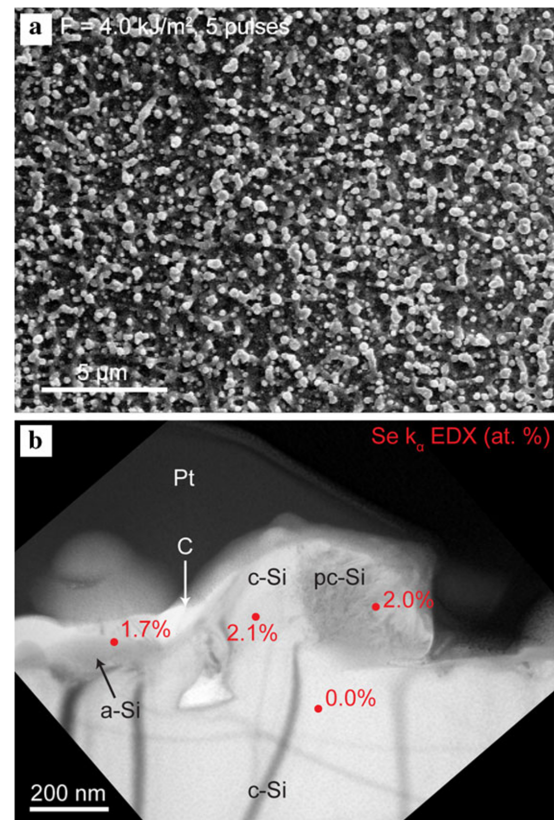

Fig. 2 (**a**) Top-view SEM image of roughened surface after 5 fs-laser pulses at $F = 4.0\ kJ/m^2$. (**b**) BF-TEM micrograph of the roughened surface showing single-crystalline, polycrystalline, and amorphous silicon contributing to surface roughness. The selenium composition (at.%) was determined using EDX (*red spots*). Platinum (Pt) and carbon (C) layers were deposited during FIB sample preparation

(Fig. 1a) shows that a single laser pulse at 4 kJ/m^2 results in significant removal of the Se film, but does not produce noticeable surface roughness on the underlying Si. As it is evident from both SEM and TEM images (Figs. 1a and 1b), much of the 75 nm Se thin film has been removed, but some Se remains on the surface (Fig. 1b). A high-magnification micrograph (Fig. 1c) shows that the native Si oxide layer stays intact after a single laser pulse at 4 kJ/m^2 and is covered by a 1-nm thick Se layer, as identified using EDX (not shown). Beneath the native oxide layer, 10 nm of amorphous Si has formed through the melting and ultrafast resolidification of Si following laser irradiation. The presence of a thin Se film above the Si oxide layer and amorphous Si beneath the oxide layer is evidence that the native layer stays intact following a single fs-laser pulse, which has also been observed following ns-pulsed laser irradiation [20].

We can contextualize the behavior of the Se thin film during fs-laser irradiation by considering the difference in material properties between Se, Si and SiO_2. Se melts at a much lower temperature (217 °C) than Si or Si dioxide, which suggests that the melting and ablation fluence thresholds during fs-laser irradiation are also significantly lower. In addition to possibly operating above the ablation threshold of Se, the evaporation temperature of Se is only 685 °C [21], and thus evaporation will also contribute to Se removal following initial pulses of fs-laser irradiation. The robust nature of the Si oxide and the low modification threshold of the thin-film dopant precursor present a considerable challenge for uniform dopant incorporation using a thin film.

With continued irradiation using multiple laser pulses, the surface exhibits considerable roughening (Fig. 2a). TEM investigations of the sample after 5 pulses (Fig. 2b) reveal that amorphous, crystalline, and polycrystalline regions have formed on the surface. EDX results indicate that there

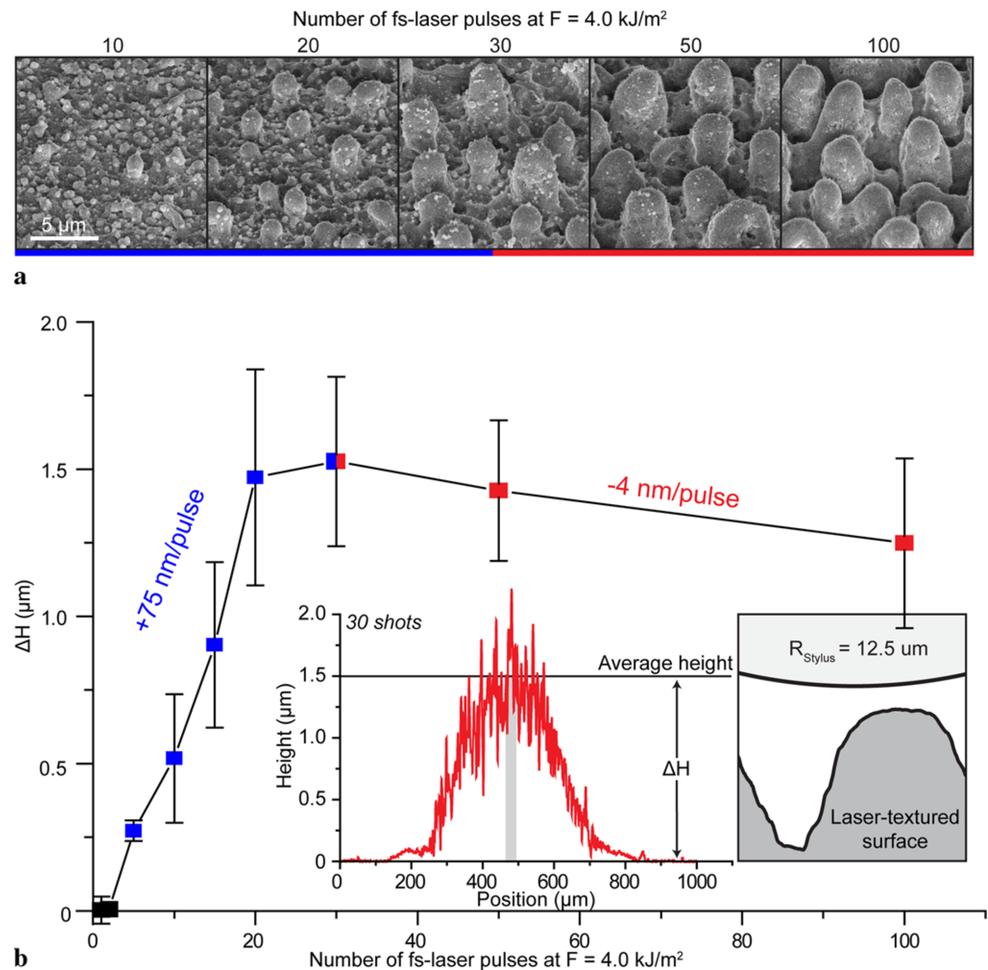

Fig. 3 (**a**) SEM images taken at 45° angle showing evolving surface morphology with increasing laser pulse number (10–100) at a fluence of 4.0 kJ/m^2. (**b**) Average height of the surface peaks with respect to the native silicon substrate (ΔH), measured using a profilometer line scan across the entire laser spot. *Inset* (*left*) shows an example profilometry line scan across a stationary laser spot irradiated with 30 pulses. The average height in the center 30 µm (*shaded*) is measured with respect to the height of the unirradiated silicon wafer and used to quantify trends in the height of the surface (ΔH) with shot number. The right inset illustrates the relative size of laser-textured surface and the profilometer stylus with 12.5 µm radius of curvature

is 1–2 % Se in the amorphous, crystalline, and polycrystalline Si regions on the surface, confirming that Se mixes with molten Si after multiple laser pulses. The detection of selenium in crystalline Si indicates that in some regions there is melting followed by epitaxial recrystallization. The amount of Se remaining on the surface is significantly less than originally deposited, as might be expected because of Se ablation/evaporation during the first several laser pulses. The native oxide layer observed in Fig. 1 might be expected to introduce O into the doped material, but such light elements are difficult to detect using EDX.

Notably, the only crystalline material that is doped is confined to within the surface protrusions, suggesting that the synthesis of crystalline doped Si and surface texturing are coupled from an early stage of laser irradiation. A roughened surface morphology could affect both the energy deposition and energy dissipation processes during fs-laser irradiation, which is known to have strong consequences on crystallization. Supporting the relationship between morphology and crystallization that we observe, Borowiec et al. investigated the microstructure of a Si surface following a single laser pulse and observed crystallization only in the protruding ring around the laser spot [22].

3.1.2 Dopant incorporation during surface texturing with 5–100 pulses at F = 4 *kJ/m*^{2}

Our investigations after 1 pulse and 5 pulses have shown that much of the Se is evaporated/ablated away during the early stages of irradiation and that the crystallization of doped Si is closely tied to surface morphology from the earliest stages of surface texturing. In order to understand how local crystallized protrusions after 5 pulses lead to the formation of large Se-rich polycrystalline peaks [12], we extend this investigation to higher pulse numbers.

The gradual texturing of the surface with an increasing number of laser pulses at a fluence of 4 kJ/m^2 is shown in Fig. 3a. It has been previously reported that irradiation conditions govern whether surface texturing occurs through material addition to the peaks or by material removal from regions between the peaks [11]. To investigate the surface texturing mechanism, we performed profilometry line scans across each laser-irradiated spot (1–100 laser pulses), such that the peak height in the center of the laser spot can be quantified with respect to the initial height of the unirradiated Si wafer (Fig. 3b, inset). The width of the profilometer

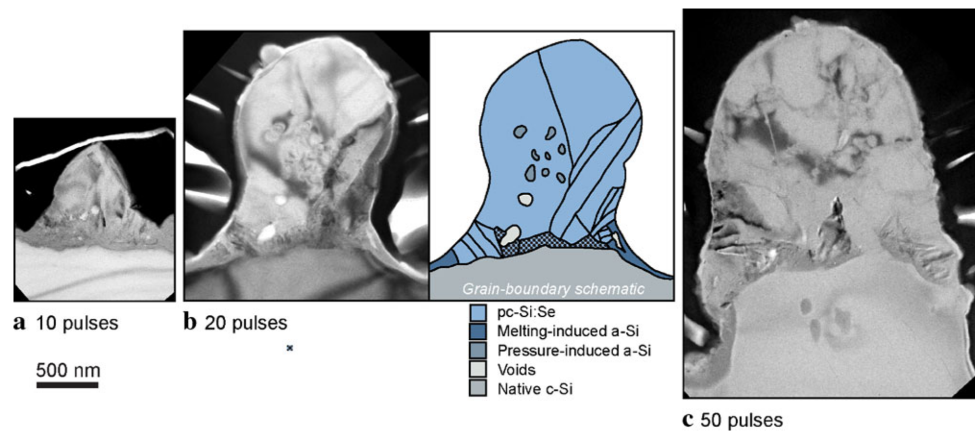

Fig. 4 BF-TEM images of polycrystalline peaks on the surface after (**a**) 10, (**b**) 20, and (**c**) 50 pulses at F = 4 kJ/m^2, all shown at the same magnification. A schematic of the grain structure of the 20-shot peak included in (**b**) shows representative distribution of grains. At the base of the peak, the grains are columnar and on the order of 100 nm, but the body of the peak is made up of several micrometer-scale grains. The *dotted areas* at the bottom of the polycrystalline peak indicate regions in which there was too much contrast to easily resolve the grain structure in a 2D schematic. We have previously reported [24, 25] the pressure-induced formation of amorphous Si, identified in the schematic

stylus prevents detecting the valleys between the peaks, but allows for extraction of the average peak height. To obtain the height of the peaks at the center of the laser spot, we averaged the height measurement across the center 30 µm of the laser modified spot (Fig. 3b). For irradiation with 5–30 laser pulses, profilometry reveals that there is upward peak growth at a rate of 75 nm/pulse between 5–30 laser pulses; this finding contrasts the case of fs-laser doping with SF_6 in which the peak growth is predominantly driven by material removal [23]. After 10 pulses, the surface peaks have grown visibly above the surrounding roughened surface (Fig. 3a), reaching 517 ± 218 nm above the native Si surface and then growing to an average height of 1472 ± 367 nm over the 10 subsequent laser pulses.

TEM characterization of representative surface peaks after 10 and 20 pulses (Figs. 4a and 4b) reveals that the peaks are polycrystalline and that the growing height of the surface peaks in this irradiation regime occurs through an increased volume of polycrystalline Si within each peak. As illustrated in the grain structure schematic in Fig. 4b, the 20-pulse peaks exhibit increasing grain size toward the center and top of the peaks, with columnar grains less than 100 nm in size at the interface of the polycrystalline and amorphous Si transitioning into grains approaching micrometer-scale dimensions in the center of the peak. These structural investigations therefore suggest that the increasing volume of the polycrystalline peaks is related to crystallization at the base of the peaks occurring in parallel with grain coarsening within the polycrystalline region with continued fs-laser irradiation.

With continued irradiation (30–100 pulses) the surface peaks continue to evolve (Fig. 3a) while the peak height relative to the unirradiated surface gradually begins to decrease (Fig. 3b). These opposite trends are evidence that peak evolution is now occurring predominantly through material removal from regions between the peaks. Supporting the transition into ablation-driven growth, investigations of the microstructure after 50 pulses (Fig. 4c) indicate that the valleys between the peaks are significantly recessed from the polycrystalline-crystalline interface. This process is well understood and is the dominant form of surface texturing during fs-laser doping from SF_6 gas [23]: laser light is preferentially reflected into the valleys between the peaks, creating localized regions of increased fluence and heightened rates of material ablation. Our investigation shows that crystallization-induced peak growth leads to the initial surface texturing, but with continued irradiation the peak amplitude increases through localized ablation.

The differences in the surface texturing processes observed during gas and thin-film fs-laser doping raises questions about the possible effects of Se impurities. Thermodynamically, the presence of impurities in Si affects the melting temperature [26] and, in turn, the volume of amorphous material that is generated. The presence of 1 % Se in a Se–Si alloy will drastically reduce the melting temperature compared to pure Si, though the magnitude of this effect is difficult to quantify. A decrease in melting temperature would increase both the melt depth and the melt duration during fs-laser irradiation [27], increasing the surface roughening during early stages of irradiation.

The presence of 0.1–1 % impurities can also have a drastic, sometimes complex effect on the crystallization kinetics of Si, depending on the crystallization mechanism. When considering liquid-phase crystallization, the presence of 1 % oxygen in amorphous Si increases the nucleation rate by a factor of 10 [28], but group III and group V impurities de-

crease the rate of nucleation when present at comparable concentrations [28]. During solid phase epitaxy, however, nondoping impurities such as O, N, and C significantly reduce the crystallization rate and electrically active group III and V dopants at concentration up to 1 % can increase the rate of solid phase epitaxy by an order of magnitude [28]. The effect of Se, a group VI dopant, might be expected to increase the kinetics similar to the group V dopants, but as Se is a nontraditional dopant for Si, this effect has not been investigated in either liquid phase or solid phase crystallization.

3.2 Achieving continuous doping using a thin-film dopant precursor

Investigations of peak formation and growth during Se thin-film fs-laser doping have shown that the dopant incorporation, surface texturing, and crystallization of doped material are closely related during irradiation at a fluence of 4 kJ/m^2 fluence. The resulting discontinuous distribution of selenium-doped crystalline Si, however, is not conducive to planar device processing and has been linked to poor p–n diode rectification [12]. Thus, we investigated the surface texturing and dopant incorporation at lower laser fluences with the ultimate goal of identifying irradiation conditions conducive to the synthesis of a continuous, crystalline doped surface layer. It is well understood that at lower fluences, ripples, and not surface peaks, form after many laser pulses [23]. These ripples, known as laser-induced periodic surface structures (LIPSS), are perpendicular to the polarization of the electric field and have a periodicity of around 500–600 nm, slightly less than the wavelength of the laser. Such *low-frequency* LIPSS [29] arise through a well-known mechanism of scattering/diffraction and subsequent local-field enhancement via interference at the surface [30, 31]. Though there is a rich history of studying the formation of these surface structures on a variety of materials, dopant incorporation from a thin film during LIPSS formation has not been previously investigated and may offer a route to achieving a more continuous dopant distribution.

To address this question, we investigate the dopant distribution following 10 and 100 laser pulses in a lower fluence range where LIPSS form instead of peaks (Figs. 5 and 6). Figure 5a shows the surface after 10 pulses at fluences of 1.3–1.7 kJ/m^2 and Fig. 5b shows cross-sectional TEM of the region that received 10 pulses at 1.3 kJ/m^2 fluence. A roughly 10-nm thick Se film remains on the surface following irradiation under these low fluence conditions. Similar to what is observed after a single laser pulse at 4 kJ/m^2 (Fig. 1b), there is a 1- to 2-nm thick layer of SiO_2 separating the Se thin film from the Si substrate. We observe a 2- to 3-nm thick layer of amorphous Si beneath the native Si oxide layer, much shallower than the 10 nm of amorphous Si

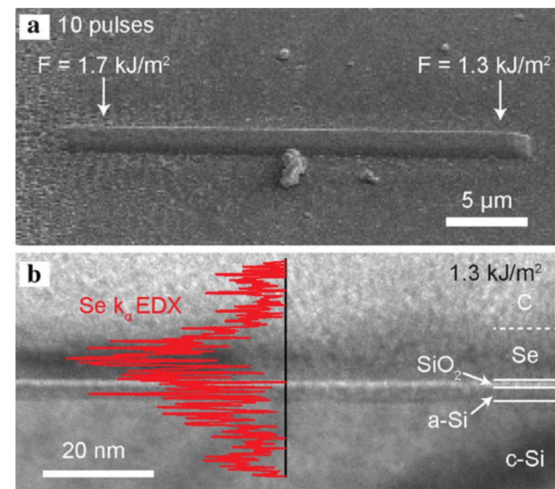

Fig. 5 (**a**) SEM image of low-fluence region (1.3–1.7 kJ/m^2) of spot irradiated with 10 laser pulses, after deposition of the protective C layer during FIB TEM sample preparation. (**b**) Cross-sectional BF-TEM of surface irradiated with 10 pulses at a fluence of 1.3 kJ/m^2 with an EDX line scan showing peak in Se signal

observed after 1 laser pulse at 4 kJ/m^2. The presence of the SiO_2 layer suggests that no Se has been incorporated into the Si after 10 pulses at 1.3 kJ/m^2. The homogeneous presence of Se at the surface, however, means the possibility of continuous Se doping may be possible with continued irradiation.

Next, we investigate Se incorporation in this same fluence regime with continued pulsed laser irradiation. Figure 6a shows the region of a laser-irradiated spot that received 100 pulses at fluences of 1.2–1.5 kJ/m^2 and exhibits LIPSS formation. A TEM micrograph of the microstructure after 100 laser pulses at 1.4 kJ/m^2 is shown in Fig. 6b. At fluences ≤ 1.4 kJ/m^2 we observe a continuous doped layer across the surface of the ripples, as confirmed by EDX (Fig. 6b). TEM micrograph of the side of a LIPSS that formed at $F = 1.25$ kJ/m^2 (Fig. 6c) confirms that the surface layer is crystalline and contains {111} stacking faults. The crystallinity and associated stacking faults are confirmed by comparing a fast-Fourier transform (FFT) from the c-Si region (Fig. 6d) with a FFT from the Se:Si layer (Fig. 6e), which exhibits a spreading in the [111] direction that is characteristic of {111} stacking faults [32]. Amorphous silicon is present above the thin recrystallized layer, though it is not continuous (Online Resource 1). Monitoring the thickness of the crystalline layer across the 1.4–1.25 kJ/m^2 range reveals that the average thickness of the doped layer increases with increasing fluence (Fig. 6f) from 11.2 ± 3.6 nm at 1.25 kJ/m^2 to 24.8 ± 12.3 nm at 1.40 kJ/m^2. At fluences higher than 1.40 kJ/m^2, we observe a transition into discontinuous polycrystalline peak formation (Online Resource 1). Based on this trend, it appears that there is an optimal fluence for thin-film doping that maximizes the thickness of

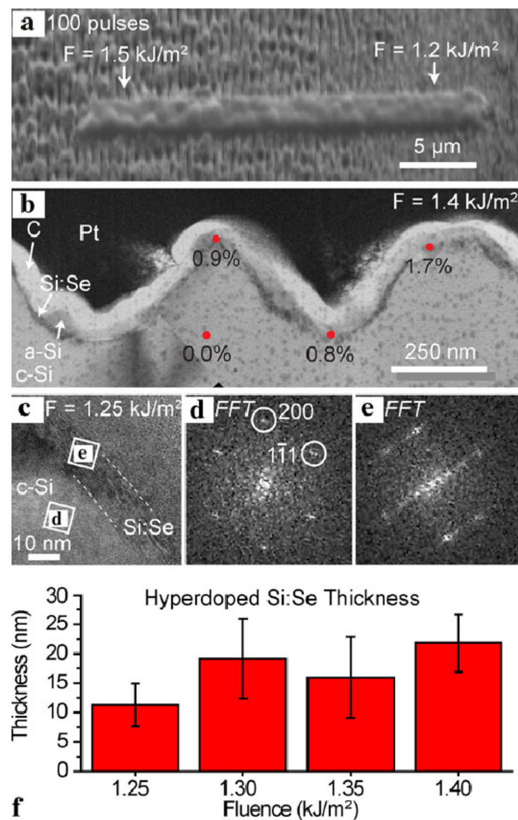

Fig. 6 (**a**) SEM image of low-fluence region (1.2–1.5 kJ/m^2) irradiated with 100 laser pulses. (**b**) BF-TEM image of surface irradiated with 100 pulses at 1.4 kJ/m^2 shows laser-induced periodic surface structures have a continuous crystalline surface layer. EDX point scans indicate selenium composition in surface layer of around 1 %. For clarity, the crystalline substrate (c-Si), hyperdoped silicon (Si:Se), amorphous silicon (a-Si), and protective coatings (C, Pt) are indicated. (**c**) BF-TEM image of Se:Si surface layer taken from the region that received 100 pulses at 1.25 kJ/m^2 (low magnification TEM image available in Online resource 1). (**d**) Indexed FFT taken from c-Si region indicated in (**c**), exhibiting pattern characteristic of the [110] zone axis. (**e**) FFT of Se:Si region exhibits spreading in the [111] direction that is characteristic of {111} stacking faults. (**f**) Thickness of the hyperdoped surface layer plotted as a function of fluence indicates increasing surface layer thickness with increasing fluence

the crystalline Se:Si surface layer while suppressing the formation of discontinuous polycrystalline peaks on the surface.

To elucidate the dopant incorporation mechanisms during LIPSS formation between 10 and 100 pulses at fluences around 1.3–1.4 kJ/m^2, we review the current understanding of fs-laser irradiation of Si in this low-fluence regime. Melting during fs-laser irradiation can occur through both thermal and nonthermal pathways and each has different thresholds; it is generally observed that the nonthermal melting threshold is around 1.5 times the fluence required for thermal melting [33]. Izawa et al. correlated nonthermal melting in Si with amorphous Si formation and, at lower fluences, correlated thermal melting with the formation of a thin layer of crystalline Si. Comparing our structural investigations with those of Izawa et al. suggests that the doped layer we observe is a consequence of thermal melting and recrystallization, which dominates only at sufficiently low fluences during fs-laser irradiation. Both ps- and ns-laser irradiation of a Se thin film on Si have been shown to produce crystalline Se-doped Si, [5, 16] inherently through thermal melting as nonthermal melting is unique to fs-laser irradiation. These investigations suggest that irradiation at sufficiently low fluences is an important criteria for achieving a continuous layer of doped c-Si from a thin-film precursor using fs-laser irradiation. Future studies will investigate the bulk properties of the Se-doped Si synthesized using pulsed laser doping with fs-laser irradiation and a thin-film precursor.

4 Conclusions

Our investigation reveals important consequences of using a thin-film dopant precursor during fs-laser doping. Irradiation of Si with many laser pulses at 4 kJ/m^2 creates micrometer-scale peaks on the surface during both the gas-phase and thin-film fs-laser doping, but there are significant differences in the surface texturing mechanisms. When using a thin-film precursor a unique regime exists between 5–30 laser pulses (at 4 kJ/m^2) during which the peaks grow rapidly upward from the surface. We have shown that high fluences ablate/evaporate the Se thin film before substantial dopant incorporation can take place and proceeds to drive localized crystallization of doped material only within protruding surface features. With this understanding, we were able to achieve more uniform dopant incorporation by moving to sufficiently low fluences, which we found to be in the range of 1.3–1.4 kJ/m^2 under these irradiation conditions. After 10 pulses, there is a layer of Se dopant precursor remaining on the surface and after 100 fs-laser pulses a continuous Se-rich crystalline layer forms in parallel with LIPSS. These systematic structural investigations elucidate the evolution of the dopant incorporation and microstructure during thin-film fs-laser doping and we can use this understanding to improve the dopant distribution, an important step toward the rational synthesis of materials using thin-film fs-laser doping.

Acknowledgements The authors acknowledge valuable discussions with Kasey Phillips. This work was supported by the Chesonis Family Foundation, the National Science Foundation (NSF) ERC-QESST (EEC-1041895), and NSF awards CBET 0754227 and CHE-DMR-DMS 0934480. This research was also made with additional support through the National Defense Science and Engineering Graduate (NDSEG) Fellowship, 32 CFR 168a, and the R.J. McElroy Trust. We acknowledge valuable use of MIT CMSE Shared Experimental Facilities, under MIT NSF MRSEC grant # DMR-08-19762, and the Harvard Center for Nanoscale Systems (CNS), a member of the National Nanotechnology Infrastructure Network (NNIN), which is supported by NSF Award No. ECS-0335765.

References

1. S.H. Pan, D. Recht, S. Charnvanichborikarn, J.S. Williams, M.J. Aziz, Appl. Phys. Lett. **98**, 121913 (2011)
2. C.H. Crouch, J.E. Carey, M. Shen, E. Mazur, F.Y. Génin, Appl. Phys. A, Mater. Sci. Process. **79**, 1635 (2004)
3. J.E. Carey, C.H. Crouch, M. Shen, E. Mazur, Opt. Lett. **30**, 1773 (2005)
4. A.J. Said, D. Recht, J.T. Sullivan, J.M. Warrender, T. Buonassisi, P.D. Persans, M.J. Aziz, Appl. Phys. Lett. **99**, 073503 (2011)
5. S. Hu, P. Han, S. Wang, X. Mao, X. Li, L. Gao, Semicond. Sci. Technol. **27**, 102002 (2012)
6. A. Luque, A. Martí, Phys. Rev. Lett. **78**, 5014 (1997)
7. M.A. Sheehy, B.R. Tull, C.M. Friend, E. Mazur, Mater. Sci. Eng. B, Solid-State Mater. Adv. Technol. **137**, 289 (2007)
8. M.J. Sher, M.T. Winkler, E. Mazur, Mater. Res. Soc. Bull. **36**, 439 (2011)
9. B.R. Tull, M.T. Winkler, E. Mazur, Appl. Phys. A, Mater. Sci. Process. **96**, 327 (2009)
10. M.T. Winkler, M.J. Sher, Y.T. Lin, M.J. Smith, H. Zhang, S. Gradečak, E. Mazur, J. Appl. Phys. **111**, 093511 (2012)
11. V. Zorba, I. Alexandrou, I. Zergioti, A. Manousaki, C. Ducati, A. Neumeister, C. Fotakis, G.A.J. Amaratunga, Thin Solid Films **453–454**, 492 (2004)
12. M.J. Smith, M.T. Winkler, M.J. Sher, Y.T. Lin, E. Mazur, S. Gradečak, Appl. Phys. A, Mater. Sci. Process. **105**, 795 (2011)
13. S. Hu, P. Han, S. Wang, X. Mao, X. Li, L. Gao, Phys. Status Solidi A **209**, 2521 (2012)
14. B.P. Bob, A. Kohno, S. Charnvanichborikarn, J.M. Warrender, I. Umezu, M. Tabbal, J.S. Williams, M.J. Aziz, J. Appl. Phys. **107**, 123506 (2010)
15. T.G. Kim, J.M. Warrender, M.J. Aziz, Appl. Phys. Lett. **88**, 3 (2006)
16. M. Tabbal, T.G. Kim, D.N. Woolf, B. Shin, M.J. Aziz, Appl. Phys. A, Mater. Sci. Process. **98**, 589 (2010)
17. A.L. Baumann, K.M. Guenther, P. Saring, T. Gimpel, S. Kontermann, M. Seibt, W. Schade, Energy Procedia **27**, 480 (2012)
18. S. Kontermann, T. Gimpel, A.L. Baumann, K.M. Guenther, W. Schade, Energy Procedia **27**, 390 (2012)
19. K. Affolter, W. Luthy, M. Von Allmen, Appl. Phys. Lett. **33**, 185 (1978)
20. G.E. Jellison Jr., D.H. Lowndes, Appl. Phys. Lett. **51**, 352 (1987)
21. M. de Selincourt, Proc. Phys. Soc. **52**, 348 (1940)
22. A. Borowiec, M. MacKenzie, G.C. Weatherly, H.K. Haugen, Appl. Phys. A, Mater. Sci. Process. **76**, 201 (2003)
23. B.R. Tull, J.E. Carey, E. Mazur, J. McDonald, S.M. Yalisove, Mater. Res. Soc. Bull. **31**, 7 (2006)
24. M.J. Smith, Y.T. Lin, M.J. Sher, M.T. Winkler, E. Mazur, S. Gradečak, J. Appl. Phys. **110**, 053524 (2011)
25. M.J. Smith, M.J. Sher, B. Franta, Y.T. Lin, E. Mazur, S. Gradečak, J. Appl. Phys. **112**, 083518 (2012)
26. M.J. Aziz, T. Kaplan, Acta Metall. **36**, 2335 (1988)
27. E.P. Fogarassy, D.H. Lowndes, J. Narayan, C.W. White, J. Appl. Phys. **58**, 2167 (1985)
28. G.L. Olson, J.A. Roth, Mater. Sci. Rep. **3**, 1 (1988)
29. J. Bonse, M. Munz, H. Sturm, J. Appl. Phys. **97**, 013538 (2005)
30. Z. Guosheng, P.M. Fauchet, A.E. Siegman, Phys. Rev. B **26**, 5366 (1982)
31. J.E. Sipe, J.F. Young, J.S. Preston, H.M. van Driel, Phys. Rev. B **27**, 1141 (1983)
32. F.J. Lopez, E.R. Hemesath, L.J. Lauhon, Nano Lett. **9**, 2774 (2009)
33. A. Cavalleri, K. Sokolowski-Tinten, J. Bialkowski, M. Schreiner, D. von der Linde, J. Appl. Phys. **85**, 3301 (1999)